profile with 2 zero-dispersion wavelengths (2-ZDW) and an all-normally dispersive profile (ANDi). Corresponding values of n_1 to n_4 for the two profiles are 1, 0.2, 0.8, and 0.6 and 0.6, 0.2, 0.3, and 0.2, respectively.

Generated SC, resulting pulse-to-pulse coherence (g_{12}) and intrapulse coherence (Γ) after 10-cm propagation are shown in Fig. 2. Here a pump wavelength of 1.55 μm was assumed. The injected peak powers for 2-ZDW and ANDi profiles are 30 and 200 kW, respectively. While all spectra in Fig. 2(a) encompass more than one octave, the coherence properties are quite different. For the 2 ZDW profile, the values of g_{12} for the 100-fs pulse approach unity in the wavelength range of interest while for the 400-fs pulses, most values are below 0.25, except for a narrow-band range around 1.6 μm, which relates to a heavily damped $2f$ component at 3.2 μm, which appears of little practical relevance. In contrast, for the ANDi profile, the values of g_{12} approach unity for both, 100 and 400-fs input pulses from 1.9 μm to 2.5 μm, as shown in Fig. 2(b). This feat is caused by the absence of the modulation instability in the ANDi region. Therefore, noise amplification is greatly suppressed during the spectrum broadening. In Fig. 2(c), intrapulse coherence manifests itself in a different manner compared to the pulse-to-pulse coherence. At 1.6 μm wavelength, Γ suddenly drops below 0.25 for the 2 ZDW profile when the input width is 100 fs. This means that spectral components larger than 3.2 μm have rather unstable phases. For the 400-fs input, instead, the situation is even worse, as intrapulse coherence is vanishing throughout the entire spectrum. In contrast, the values of Γ for ANDi profile are nearly 1 in a much broader range because noise amplification induced by the modulation instability is nearly completely mitigated.

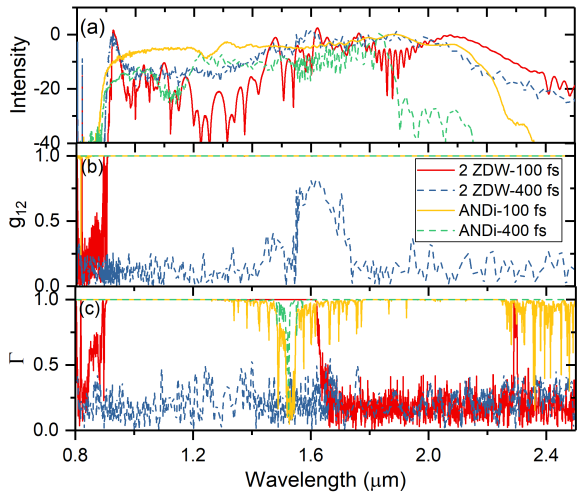

Fig. 2. Resulting (a) SC, (b) pulse-to-pulse coherence and (c) intrapulse coherence for the 2-ZDW profile for 100-fs input pulses (red solid curves) and 400-fs input pulses (blue dashed curves). In addition, curves are shown for the ANDi profile (100-fs input, yellow solid curves) and 400-fs input (green dashed curves). Pump wavelength for all cases was assumed as 1.55 μm

We further ran numerical simulations to clarify the break-up of coherence with propagation distance z. As can be seen from Fig. 3(a), intrapulse coherence quickly approaches unity within 2 cm, when the input width is 100 fs. In contrast, when the pulse width is increased to 400 fs, intrapulse coherence significantly degrades at similar length scales. This means longer pulse is rather unsuitable for obtaining high intrapulse coherence with a 2-ZDW profile. However, resultant patterns for ANDi profile appear much more promising, regardless of whether the input duration is 100 or 400 fs. In particular, the coherent bandwidth occupied by high intrapulse coherence is much broader. Moreover, intrapulse coherence already reaches its maximum value within much shorter propagation, e.g., when the input width is 100 fs. We therefore conclude that ANDi profiles exhibit an obvious edge compared to rather conventional 2-ZDW profiles, which pay out in a high intrapulse coherence. Nevertheless, this edge does not come without a price to pay, i.e., significantly higher input peak powers are required to warrant this apparent advantage in terms of coherence.

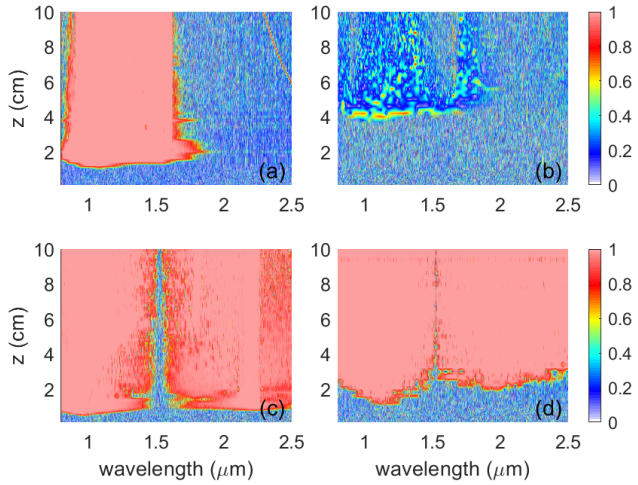

Fig. 3. Evolution of intrapulse coherence along propagation under the conditions of (a) 2-ZDW with 100 fs duration, (b) 2-ZDW with 400 fs duration, (c) ANDi with 100 fs duration, and (d) ANDi with 400 fs duration

REFERENCES

[1] E. Goulielmakis, E. Uiberacker, R. Kienberger, A. Baltuska, V. Yakovlev *et al.*, "Direct measurement of light waves," *Science*, vol. 305, pp. 1267–1269, Aug. 2004.

[2] H. R. Telle, G. Steinmeyer, A. E. Dunlop, J. Stenger, D. H. Sutter *et al.*, "Carrier-envelope offset phase control: a novel concept for absolute optical frequency measurement and ultrashort pulse generation," *Appl. Phys. B*, vol. 69, pp. 327–332, Feb. 1999.

[3] J. M. Dudley, G. Genty, and S. Coen, "Supercontinuum generation in photonic crystal fiber," *Rev. Mod. Phys.*, vol. 78, pp. 1135–1184, Oct. 2006.

[4] Y. Zhang, J. Kainerstorfer, J. C. Knight, and F. G. Omenetto, "Experimental measurement of supercontinuum coherence in highly nonlinear soft-glass photonic crystal fibers," *Opt. Express*, vol. 25, pp. 11 842–11 852, Aug. 2017.

[5] G. Genty, P. Kinsler, B. Kibler, and J. Dudley, "Nonlinear envelope equation modeling of sub-cycle dynamics and harmonic generation in nonlinear waveguides,," *Opt. Express*, vol. 15, pp. 5382–5387, Apr. 2007.

[6] R. Liao, C. Mei, Y. Song, A. Demircan, and G. Steinmeyer, "Spontaneous emission noise in mode-locked lasers and frequency combs," *Phys. Rev. A*, vol. 102, pp. 013 506–1–12, Jul. 2020.